In vitro apatite formation and drug loading/release of porous TiO_2 microspheres prepared by sol-gel processing with different SiO_2 nanoparticle contents

Masakazu Kawashita[1], Yui Tanaka[1], Shoji Uneno[1], Gengci Liu[1], Zhixia Li[2], Toshiki Miyazaki[3]

[1] Graduate School of Biomedical Engineering, Tohoku University, Sendai 980-8579, Japan

[2] School of Chemistry and Chemical Engineering, Guangxi University, Nanning 530004, China

[3] Graduate School of Life Science and Systems Engineering, Kyushu Institute of Technology, Kitakyushu 808-0196, Japan

Corresponding author: Masakazu Kawashita

E-mail: m-kawa@ecei.tohoku.ac.jp

TEL: +81-22-795-3937, FAX: +81-22-795-4735

Abstract

Bioactive titania (TiO_2) microparticles can be used as drug-releasing cement fillers for the chemotherapeutic treatment of metastatic bone tumors. Porous anatase-type TiO_2 microspheres around 15 μm in diameter were obtained through a sol-gel process involving a water-in-oil emulsion with 30:70 SiO_2/H_2O weight ratio and subsequent NaOH solution treatment. The water phase consisted of methanol, titanium tetraisopropoxide, diethanolamine, SiO_2 nanoparticles, and H_2O, while the oil phase consisted of kerosene, Span 80, and Span 60. The resulting microspheres had a high specific surface area of 111.7 $m^2 \cdot g^{-1}$. Apatite with a network-like surface structure formed on the surface of the microspheres within 8 days in simulated body fluid. The good apatite-forming ability of the microspheres is attributed to their porous structure and the negative zeta potential of TiO_2. The release of rhodamine B, a model for a hydrophilic drug, was rapid for the first 6 h of soaking, but diffusion-controlled thereafter. The burst release in the first 6 h is problematic for clinical applications; nonetheless, the present results highlight the potential of porous TiO_2 microspheres as drug-releasing cement fillers able to form apatite.

Keywords: TiO_2, Microsphere, Apatite, Rhodamine B, Bioactivity, Drug-release

1 Introduction

Lung cancer, breast cancer and prostate cancer often metastasize to bone [1]. Metastatic bone tumors are not fatal, but often cause skeletal pain and pathological fractures resulting in a marked decrease in patients' quality of life. Metastatic bone tumors are usually treated with a combination of surgical operations and chemotherapy. Firstly, the cancer-affected region is extirpated by surgery and the excision site is sometimes filled with injectable calcium phosphate cement in order to achieve early postoperative ambulation [2–4]. After the surgical operation, chemotherapy is performed in order to prevent cancer recurrence and metastasis. However, chemotherapy often carries a risk of side effects because the drugs are often administered systemically.

Polymethylmethacrylate (PMMA) and calcium phosphate cements are useful fillers for the excision site because of their excellent mechanical properties. PMMA cement is usually encapsulated by fibrous tissues and cannot bond to living bone, i.e. show bioactivity, if the matrix does no contain titania (TiO_2) nano- or microparticles [5, 6] whose apatite-forming ability is responsible for the bioactivity of the cement. TiO_2 particles able to release drugs would therefore confer both bioactivity and chemotherapeutic abilities to PMMA cement. Previously, Yamashita et al. reported that porous TiO_2 microspheres approximately 5 μm in diameter can be obtained using a sol-gel method with a water-in-oil (W/O) emulsion [7, 8]. In this sol-gel approach, colloidal silica (SiO_2) nanoparticles are firstly incorporated into TiO_2 microspheres and then leached out with a sodium hydroxide (NaOH) aqueous solution leaving behind a porous structure. We recently investigated the effects of SiO_2 nanoparticle size (15, 50, or 200 nm) on the apatite-forming ability of porous TiO_2 microspheres in simulated body fluid (SBF), and found that pore size and pore shape are important factors influencing the formation of apatite [9]. However, the effects of the SiO_2 nanoparticle content on the formation of apatite on the porous TiO_2 microspheres in SBF and the drug-releasing ability of the porous TiO_2 microspheres were not investigated. In this study, in order to evaluate the potential of porous TiO_2 microspheres as apatite-forming, drug-releasing cement fillers, we investigated first, the apatite-forming ability of porous TiO_2 microspheres prepared with different SiO_2 nanoparticle contents, and second, the drug-releasing behavior of the porous TiO_2 microspheres by using rhodamine B as a model for a hydrophilic drug [10, 11].

2 Experimental procedures

2.1 Sample preparation

All of the reagent-grade chemicals were purchased from Wako Pure Chemical Industries, Tokyo, Japan. Porous TiO_2 microspheres were prepared using a sol-gel method in W/O emulsion, based on our previous study [9]. For the oil phase, kerosene (54.0 g), Span80 (9.0 g), and Span60 (3.0 g) were mixed at 40 °C for 15 min in a homogenizer (HG-200, AS ONE Corp., Osaka, Japan) at 1800 rpm. For the water phase, methanol (2.7 g), titanium tetraisopropoxide (3.36 g), and diethanolamine (2.0 g) were mixed at 0 °C with a magnetic stirrer (HS-360, AS ONE Corp., Osaka, Japan).

Separately, SiO_2 nanoparticle suspensions with varying SiO_2 contents were prepared by adding different amounts of colloidal SiO_2 (Snowtex® XL, Nissan Chemical Industries, Ltd., Tokyo, Japan) to ultrapure water (H_2O). The average size and concentration of the SiO_2 nanoparticles in the colloid were 50 nm and 40 wt%, respectively. The total H_2O content of the dispersion was fixed at 4.2 g by changing the amount of H_2O added. Table 1 gives the sample names, the corresponding SiO_2 and H_2O contents, and the SiO_2/H_2O weight ratios in the SiO_2 nanoparticle dispersions. The number in the sample name (S-*xx*) indicates its SiO_2 content (wt%). The SiO_2 nanoparticle dispersion was mixed with the water phase and then dropped into the oil phase under continuous mixing in the homogenizer to achieve a W/O emulsion. The mixing was prolonged at 40 °C for 20 min at 1800 rpm, at 50 °C for 20 min at 1800 rpm, at 60 °C for 70 min at 1800 rpm, and finally at 60 °C for 70 min at 1700 rpm. After mixing, the W/O emulsion was centrifuged at 3000 rpm for 5 min (CN-1050, AS ONE Corp., Osaka, Japan) and the supernatant liquid was removed by decantation. The precipitates were twice washed with 30 mL of ethanol, dried at 60 °C for 12 h, and then heat-treated at 600 °C for 5 h in an electric furnace (FO100, Yamato Scientific Co., Ltd., Tokyo, Japan), with the temperature increased at a rate of 5 °C·min^{-1}.

To create porous structures, the heat-treated precipitates prepared with 0:100 or 10:90 weight ratios of SiO_2/H_2O were soaked in 4 mL of 3 mol·L^{-1} (M) sodium hydroxide (NaOH) solution, while those with SiO_2/H_2O weight ratios of 20:80 or 30:70 were soaked in 4 mL of 1 M NaOH solution at room temperature for 24 h.

2.2 Characterization of the samples

The morphology of the samples was observed by scanning electron microscopy (SEM; VE-8800, Keyence Corp.,

Osaka, Japan). The measurements were performed in standard SEM imaging mode, at an accelerating voltage of 2 kV and a working distance of 8 mm. The samples were not pre-coated with electrically conductive materials prior to observation. The crystalline phases of the samples were investigated by powder X-ray diffraction (XRD; MiniFlex600HDA, Rigaku Corp., Tokyo, Japan), with a Cu Kα source operating at 40 kV-15 mA and with a scanning rate of 10 °·min^{-1}. The structures of the samples were investigated by Fourier-transformed infrared spectroscopy (FT-IR; FT/IR-6200, JASCO Corp., Tokyo, Japan), by recording transmission spectra using the potassium bromide (KBr) pellet method. The KBr content of the testing samples was kept at around 0.125 wt%. The specific surface area (SSA) of the samples was measured with a gas absorption analyzer (Autosorb®-iQ-C, Quantachrome Corp., Florida, USA), and the pore size distribution in sample S-30 before and after NaOH solution treatment was derived from volumetric adsorption measurements (BELSORP-mini II, BEL Japan, Osaka, Japan). The samples were heated at 200 °C for 2 h prior to measurements in order to remove adsorbed water. The zeta potentials of the samples were measured by laser electrophoresis spectroscopy (ZS90, Malvern Instruments Ltd., Worcestershire, UK) at pH 7.4 in saline. The pH of the saline was adjusted using 10 mM aqueous solutions of HCl and NaOH.

2.3 Soaking of the samples in SBF

The SBF was prepared by dissolving reagent-grade chemicals in ultrapure water according to the ISO23317:2012 protocol. All chemicals used for the preparation of SBF were purchased from Nacalai Tesque, Inc., Kyoto, Japan. Different amounts of the samples (S-0: 47.3 mg, S-10: 7.5 mg, S-20: 6.4 mg, S-30: 6.1 mg) were soaked statically in 50 mL SBF at 36.5 °C for 8 days. The different amounts used for each sample ensured matching surface areas. The SBF was refreshed every two days.

2.4 Evaluation of rhodamine B loading and release for sample S-30

Rhodamine B adsorption and release was evaluated for sample S-30 as outlined in a previous study [10]. A total of 2.5 mg of Sample S-30 was soaked in a microtube containing 1 mL of a 0.5 mg·mL^{-1} rhodamine B solution, whose concentration was determined by the solubility of rhodamine B in water. The microtube was rotated at 3 rpm for different periods ranging from 1 to 12 h, with a tube rotator (TR-350, AS ONE Corp., Osaka, Japan). After a given period, the sample was removed from the rhodamine B solution by centrifugation at 3000 rpm for

5 min (CN-1050, AS ONE Corp., Osaka, Japan) and the rhodamine B concentration in the supernatant was measured by spectrophotometry (PD-303S, APEL Co., Ltd., Saitama, Japan). The amount of rhodamine B loaded into sample S-30 was calculated from the rhodamine B concentration in the supernatant.

After washing the sample with 1 mL of ultrapure water at the end of the 12 h experimental period, the resulting rhodamine B-loaded S-30 sample was soaked in 1 mL of ultrapure water in a microtube that was then rotated with a tube rotator at 3 rpm for different periods ranging from 1 to 96 h. After a given period, the sample was extracted by centrifugation, and the amount of rhodamine B in the supernatant was measured by spectrophotometry. Six S-30 samples were subjected to these evaluations.

3 Results and discussion

Fig. 1 shows SEM images of the different samples. Microspheres around 8 μm in diameter with smooth surfaces are observed for sample S-0 while marginally larger ones, approximately 10 μm in diameter with slightly rough surfaces are observed for samples S-10 and S-20. For sample S-30, the microspheres are around 15 μm in diameter with slightly rough surfaces. These results indicate that the incorporation of SiO_2 nanoparticles during preparation increases the size of the resultant microspheres, possibly due to the increased viscosity of the sol solution. The rough surfaces of samples S-10, S-20, and S-30 are formed by the dissolution of SiO_2 nanoparticles in the NaOH solution.

Figs. 2a and 2b respectively show XRD patterns obtained from samples before and after NaOH solution treatment, in which strong diffraction peaks ascribed to anatase (PDF: 21-1272) are observed for all samples. In addition, small diffraction peaks associated with rutile (PDF: 21-1276) are visible in the spectrum for sample S-0, while for samples S-10, S-20 and S-30, a broad peak ascribed to amorphous colloidal SiO_2 [13] is observed around $2\theta = 22°$ before NaOH treatment (Fig. 2a) and also after (Fig 2b) for the latter two samples. This suggests that for samples S-20 and S-30, some of the additive SiO_2 nanoparticles still remain even after soaking in a 1 M NaOH solution. Higher concentrations of NaOH are expected to better dissolve the SiO_2 nanoparticles, but soaking samples S-20 and S-30 in 1.5 M or 3 M NaOH solution resulted in the fracture of some of the microspheres (data not shown). One speculates that at higher NaOH concentrations, aggregates of SiO_2 nanoparticles are dissolved in the microspheres resulting in their fracture. It is noteworthy that the anatase diffraction peaks obtained for samples S-20 and S-30 are broader and less intense than those recorded for

samples S-0 and S-10, and that rutile is not formed in samples S-10, S-20, or S-30. These results indicate that the anatase phase precipitated in samples S-20 and S-30 is less crystalline than in S-0 and S-10 and that the incorporation of SiO_2 nanoparticles inhibits the phase transition from anatase to rutile. This phase transition occurs via direct formation on the surface of TiO_2 particles and/or via the nucleation of rutile points in direct contact with anatase particles [14]. Here, the SiO_2 nanoparticles might stabilize the surface of the TiO_2 particles to suppress the direct formation thereon of rutile and/or might prevent anatase particles coming into direct contact [14, 15].

Figs. 3a and 3b respectively show FT-IR spectra obtained from the samples before and after NaOH solution treatment. Absorption bands ascribed to Si-O-Si are observed at around 1100, 1020, 800, and 480 cm^{-1} for samples S-10, S-20, and S-30 before NaOH solution treatment [16], that remain visible in Fig. 3b for the latter two samples. These results indicate, in agreement with those derived from Fig. 2, that the SiO_2 nanoparticles added to sample S-10 are completely dissolved by the NaOH treatment, but a small proportion of these remain in samples S-20 and S-30 even after treatment. Furthermore, weaker absorption bands ascribed to Si-OH are observed at around 950 cm^{-1} for samples S-20 and S-30 [16], suggesting that in these samples, Si-OH groups form on the surface of the remaining SiO_2 nanoparticles.

Fig. 4 shows distributions of pore sizes in sample S-30 before and after NaOH solution treatment, and reveals that the NaOH solution treatment leads to a general increase in the pore size, probably due to the dissolution of SiO_2 nanoparticles. Note that the effect of the SiO_2 nanoparticle content on pore size distributions will be the subject of a future study.

Table 2 lists the SSA and zeta potential obtained for each sample. Samples S-10, S-20, and S-30 have remarkably higher SSAs than sample S-0, which suggests that a porous structure was successfully formed in the former samples. The SSA increases with the SiO_2 nanoparticle content as expected, but the difference in SSA between samples S-20 and S-30 is relatively small. This might be because the SiO_2 nanoparticles were not completely dissolved by soaking in the NaOH solution for these samples, as mentioned above regarding the experimental results in Figs. 2 and 3. The (negative) zeta potentials measured for these samples range from −31.2 to −26.2 mV, with those for samples S-20 and S-30 being lower than that of sample S-10 because of the presence of residual SiO_2, which has a lower zeta potential than TiO_2 [17].

Fig. 5 shows SEM images of the samples obtained after soaking in SBF. Precipitates with a network-like

surface structure are observed, in greater number for sample S-30 than for the others. Fig. 6 shows the XRD patterns recorded for the same samples. The hydroxyapatite (PDF #1-071-5048) peaks observed in all of the diffraction patterns are most intense for sample S-30, in good agreement with the images in Fig. 5. The good apatite-forming ability of sample S-30 in SBF is attributed to its porous structure [18] and the negative zeta potential of TiO_2, which contributes to the electrostatic attraction of Ca^{2+} ions from SBF [19]. Also, the Si-OH groups, which, as suggested by the FT-IR results in Fig. 3, form on the residual SiO_2 nanoparticles during soaking in NaOH solution, may also contribute to apatite formation [20]. Elsewhere, anatase and/or rutile have been shown to form during chemical and thermal treatments on titanium and titanium alloys whose apatite-forming ability was associated with the magnitude of the positive or negative zeta potentials [19, 21–23]. Here however, the apatite-forming ability of sample S-30 is apparently higher than that of sample S-0 despite their zeta potentials being almost identical (S-0: −29.9 mV and S-30: −31.2 mV). This suggests that the apatite-forming ability of the present samples is affected more by crystallinity or porosity than by the zeta potential [9]. Our previous study [9] also suggests that pore size might affect the apatite-forming ability of these materials and this will be investigated more extensively in the future.

The biological response of PMMA cement containing sample S-30 as well as the cytotoxicity of sample S-30 are interesting in the context of potential clinical applications. It is reasonable to assume that S-30-containing PMMA cement can bond to living bone in vivo. Indeed, PMMA cement containing TiO_2 nanoparticles (average particle size: 200 nm) and TiO_2 microparticles (average particle size: 1.55 μm) have been shown to bond to bone directly without fibrous capsulation [5, 6]. Besides, artificial materials that form apatite in SBF can also do so in vivo and bond to living bone trough the apatite [24].

Fig. 7 shows that the amount of rhodamine B loaded into sample S-30 increases up to 10.7 $mg \cdot g^{-1}$ for soaking times up to 12 h, but then decreases slightly after 18 h of soaking. This indicates that the maximum loading of sample S-30 with rhodamine B is obtained for a soaking time of 12 h.

Fig. 8 shows the cumulative amount of rhodamine B released from sample S-30. Rhodamine B is released rapidly for soaking times up to 6 h but more gradually thereafter. Approximately 63 % of the loaded rhodamine B is released from the sample after soaking for 96 h. Sample S-30 is negatively charged in aqueous conditions (see Table 2) and since rhodamine B is a cationic dye it may be adsorbed electrostatically on sample S-30. Plotting the amount of rhodamine B released as a function of the square root of time reveals a linear correlation

for soaking times longer than 6 h, with a high coefficient of determination (R^2, see Fig. 9). This indicates that the release of rhodamine B is diffusion-controlled for soaking times longer than 6 h [25]. The burst release in the first 6 h is undesirable for clinical applications and is a problem to be solved in the future. The pore size of the microspheres should affect the loading and release of drugs and this can be adjusted by using SiO_2 nanoparticles with different sizes [9]. However, since only sample S-30 was amenable to pore size measurements, the results of the present study are insufficient to discuss this effect, and further investigations are required. Future studies should also concentrate on the release profile of PMMA cement containing sample S-30, since sample S-30 may be covered with PMMA when it is used as cement filler. It should be noted however that previous studies suggest that TiO_2 cement fillers remain partially exposed through the PMMA [5, 6], such that it is reasonable to assume that the present rhodamine B release tests to indeed reveal the potential of sample S-30 as a drug-releasing cement filler. The release profile could furthermore be improved by adjusting the pore size and/or the zeta potential of microspheres, but the present results suggest that porous TiO_2 microspheres are potentially valuable apatite-forming carriers of hydrophilic and cationic drugs.

4 Summary

Porous TiO_2 microspheres were obtained by leaching the SiO_2 out of sol-gel-prepared SiO_2-containing TiO_2 microspheres into a NaOH solution. Porous anatase-type TiO_2 microspheres approximately 15 µm in diameter were formed with a 30:70 SiO_2/H_2O weight ratio. The incorporation of SiO_2 nanoparticles inhibits the phase transition from anatase to rutile. Apatite formed within 8 days on the surfaces of porous anatase-type TiO_2 microspheres soaked in SBF. The apatite-forming ability of the microspheres is attributed to their porous structure and the negative zeta potential of both TiO_2 and the Si-OH groups that, these results suggest, form on the residual SiO_2 nanoparticles. The release of rhodamine B, a model for a hydrophilic drug, was rapid for the first 6 h, but diffusion controlled for soaking times longer than 6 h. The burst release in the first 6 h is a problem to be solved for clinical applications, but the present results highlight the potential of these porous TiO_2 microspheres as drug-releasing cement fillers with apatite-forming ability.

Acknowledgements We thank Dr. T. Ogawa, Tohoku University, for the zeta potential measurements, Dr. T. Yokoi, Tohoku University, for the FT-IR measurements, and Dr. H. Maeda, Nagoya Institute of Technology, for

the SSA and pore size distribution measurements. This work was partially supported by a research grant from the Hitachi Metals and Materials Science Foundation, Tokyo, Japan and the Magnetic Health Science Foundation, Fukuoka, Japan.

References

[1] R.E. Coleman, Cancer. Treat. Rev. 21 (2001) 165–176.

[2] A. Matsumine, K. Kusuzaki, T. Matsubara, A. Okamura, N. Okuyama, S. Miyazaki, K. Shintani, A. Uchida, J. Surg. Oncol. 93 (2006) 212–220.

[3] A. Matsumine, K. Kusuzaki, T. Matsubara, K. Shintani, H. Satonaka, T. Wakabayashi. S. Miyazaki, K. Morita, K. Takegami, A. Uchida, Clin. Exp. Metas. 24 (2007) 191–200.

[4] A. Matsumine, K. Takegami, K. Asanuma, T. Matsubara, T. Nakamura, A. Uchida, A. Sudo, Int. J. Clin. Oncol. 16 (2011) 101–108.

[5] K. Goto, J. Tamura, S. Shinzato, S. Fujibayashi, M. Hashimoto, M. Kawashita, T. Kokubo, T. Nakamura, Biomaterials 26 (2005) 6496–6505.

[6] K. Goto, M. Hashimoto, H. Takadama, J. Tamura, S. Fujibayashi, K. Kawanabe, T. Kokubo, T. Nakamura, J. Mater. Sci.: Mater. Med. 19 (2008) 1009–1016.

[7] H. Yamashita, K. Nozaki, K. Toshinari, T. Mima, T. Maekawa, J. Ceram. Soc. Japan 106 (1998) 1184–1189.

[8] H. Yamashita, Y. Ogawa, T. Maekawa, Bunsekikagaku 56 (2007) 511–514.

[9] Z. Li, T. Miyazaki, M. Kawashita, J. Ceram. Soc. Japan 121 (2013) 782–787.

[10] R. Zhang, M. Hummelgård, G. Lv, H. Olin, Carbon 49 (2011) 1126–1132.

[11] P. Nadrah , U. Maver, A. Jemec, T. Tišler, M. Bele, G. Dražić, M. Benčina, A. Pintar, O. Planinšek, M. Gaberščček, ACS Appl. Mater. Interfaces 5 (2013) 3908–3915.

[12] G. Wang, A.N. Otuonye, E.A. Blair, K. Denton, Z. Tao, T. Asefa, J. Solid State Chem. 182 (2009) 1649–1660.

[13] S.Y. Chang, L. Liu, S.A. Asher, J. Am. Chem. Soc. 116 (1994) 6739–6744.

[14] Y. Suyama, A. Kato, J. Ceram. Soc. Japan 86 (1978) 119–125.

[15] K. Okada, N. Yamamoto, Y. Kameshima, A. Yasumori, K.J.D. MacKenzie, J. Am. Ceram. Soc. 84 (2001)

1591–1596.

[16] G. Orcel, J. Phalippou, L.L. Hench, J. Non-Cryst. Solids 88 (1986) 114–130.

[17] P. Wilhelm, D. Stephan, J. Colloid Interf. Sci. 293 (2006) 88–92.

[18] M. Keshmiri, T. Troczynski, J. Non-Cryst. Solids 324 (2003) 289–294.

[19] H.M. Kim, T. Himeno, M. Kawashita, J.H. Lee, T. Kokubo, T. Nakamura, J. Biomed. Mater. Res. 67A (2003) 1305–1309.

[20] P. Li, C. Ohtsuki, T. Kokubo, K. Nakanishi, N. Soga, K. de Groot, J. Biomed. Mater. Res. 28 (1994) 7–15.

[21] T. Kokubo, D.K. Pattanayak, S. Yamaguchi, H. Takadama, T. Matsushita, T. Kawai, M. Takemoto, S. Fujibayashi, T. Nakamura, J. R. Soc. Interface 7 (2010) S503–S513.

[22] D.K. Pattanayak, S. Yamaguchi, T. Matsushita, T. Kokubo, J. Mater. Sci.: Mater. Med. 22 (2011) 1803–1812.

[23] D.K. Pattanayak, S. Yamaguchi, T. Matsushita, T. Nakamura, T. Kokubo, J. R. Soc. Interface 9 (2012) 2145–2155.

[24] T. Kokubo, H. Takadama, Biomaterials, 27 (2006) 2907–2915.

[25] T. Miyazaki, T. Inoue, Y. Shirosaki, M. Kawashita, T. Matsubara, A. Matsumine, J. Biomater. Appl. 29 (2014) 543–547.

Figure and table captions

Fig. 1 Scanning electron micrographs obtained from SiO_2-containing TiO_2 microsphere samples (S-*xx*, with *xx* indicating the SiO_2 content in wt%) after NaOH solution treatment.

Fig. 2 X-ray diffraction patterns obtained from SiO_2-containing TiO_2 microsphere samples (S-*xx*, with *xx* indicating the SiO_2 content in wt%) (a) before and (b) after NaOH solution treatment.

Fig. 3 Fourier transform infrared spectra obtained from SiO_2-containing TiO_2 microsphere samples (S-*xx*, with *xx* indicating the SiO_2 content in wt%) (a) before and (b) after NaOH solution treatment.

Fig. 4 The distribution of pore sizes in the TiO_2 microsphere sample containing 30 wt% SiO_2 before and after NaOH solution treatment.

Fig. 5 Scanning electron micrographs obtained from SiO_2-containing TiO_2 microsphere samples (S-*xx*, with *xx* indicating the SiO_2 content in wt%) after soaking in simulated body fluid for 8 days.

Fig. 6 X-ray diffraction patterns obtained from SiO_2-containing TiO_2 microsphere samples (S-*xx*, with *xx* indicating the SiO_2 content in wt%) after soaking in simulated body fluid for 8 days.

Fig. 7 Amount of rhodamine B loaded into TiO_2 microsphere samples containing 30 wt% SiO_2 as a function of the soaking time in 1 mL of a 0.5 $mg \cdot mL^{-1}$ rhodamine B solution.

Fig. 8 Cumulative amount of rhodamine B released from TiO_2 microsphere samples containing 30 wt% SiO_2 as a function of the soaking time in 1 mL of ultrapure water.

Fig. 9 Cumulative amount of rhodamine B released from TiO_2 microsphere samples containing 30 wt% SiO_2 as a function of the square root of the soaking time in 1 mL of ultrapure water.

Table 1 Sample names and the corresponding colloidal SiO_2 contents, H_2O contents and SiO_2/H_2O ratios in the SiO_2 nanoparticle suspensions.

Table 2 The specific surface area and zeta potential measured for SiO_2-containing TiO_2 microsphere samples (S-*xx*, with *xx* indicating the SiO_2 content in wt%).

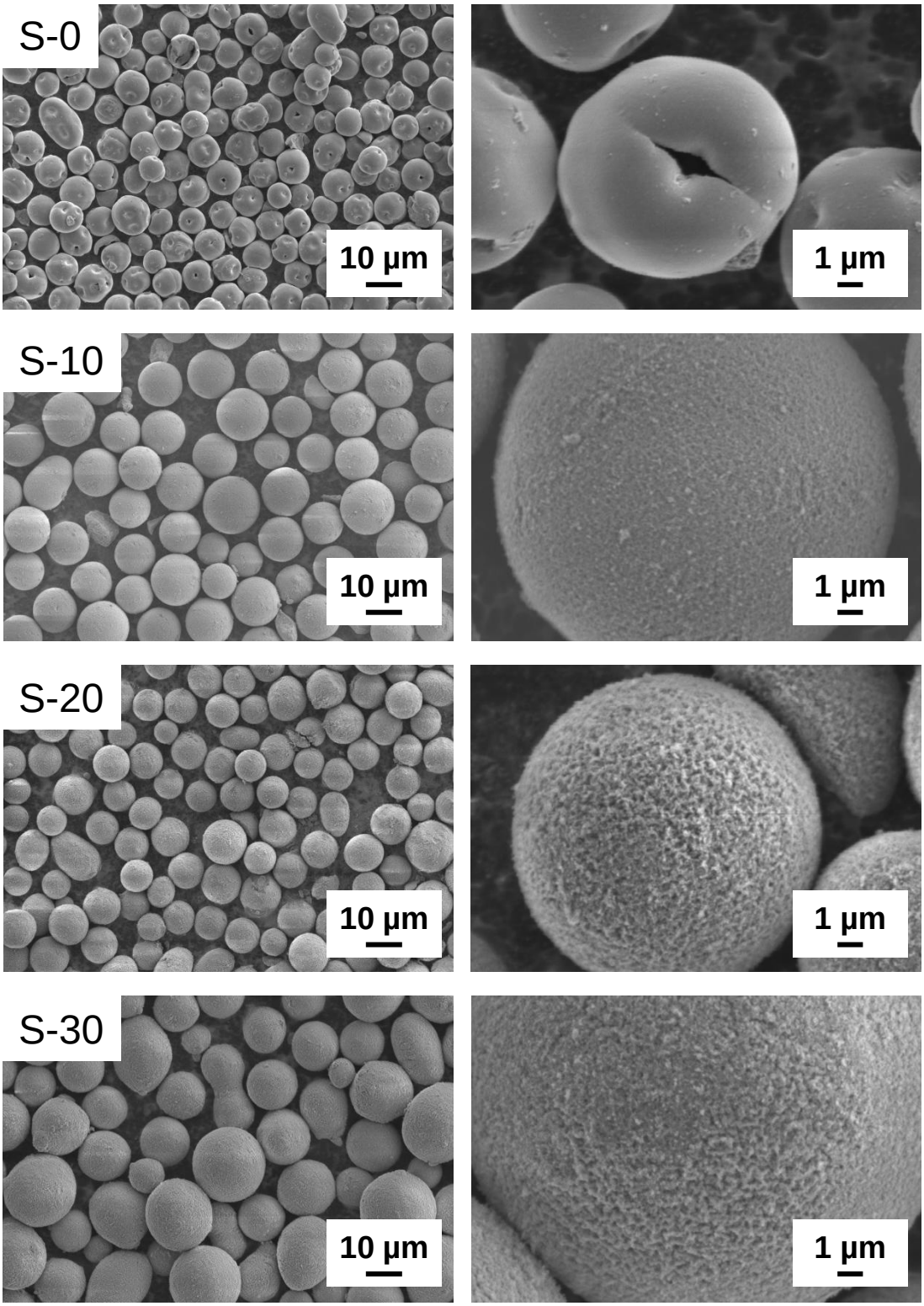

Figure 1
M. Kawashita *et al.*

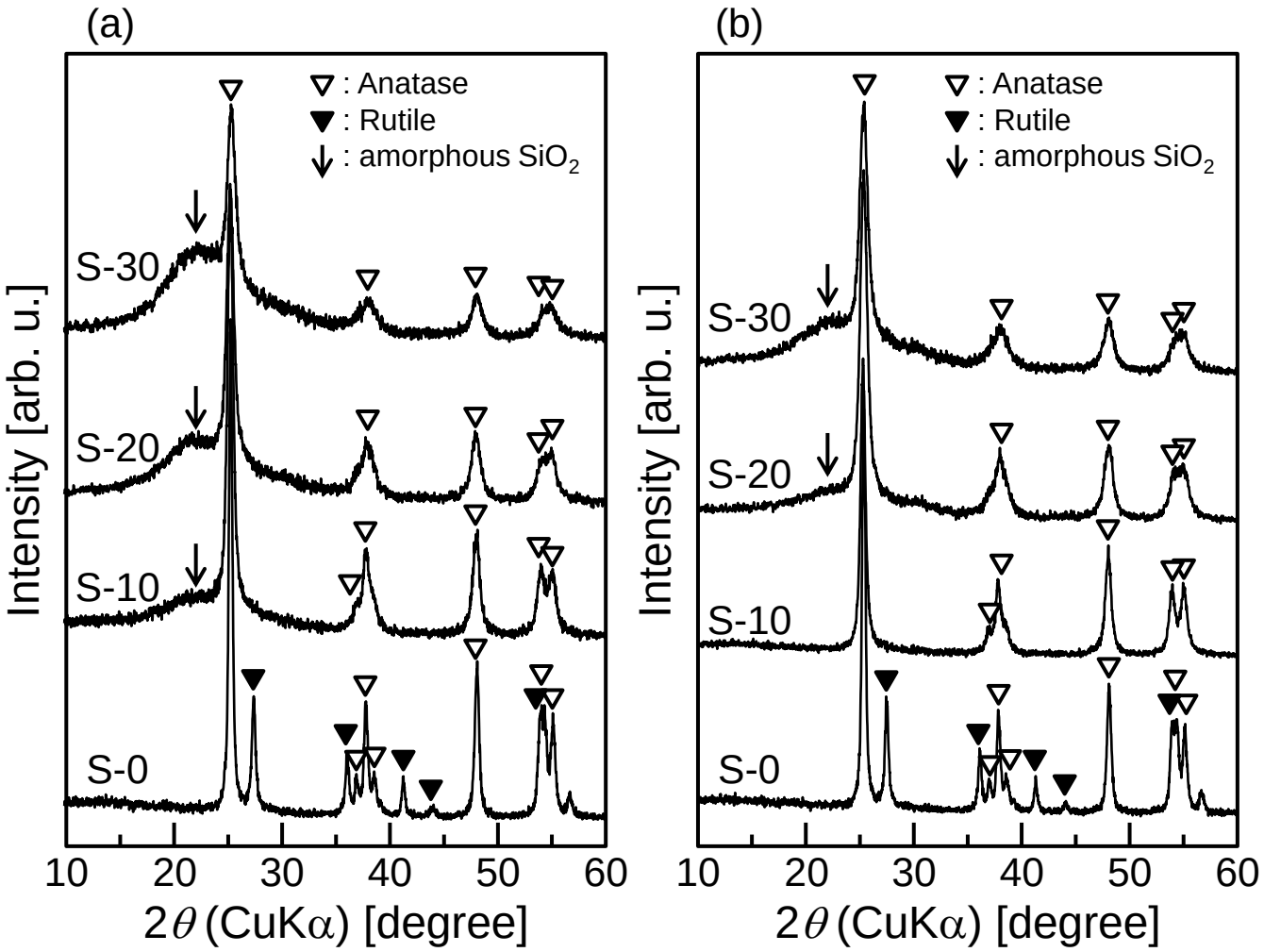

Figure 2
M. Kawashita *et al.*

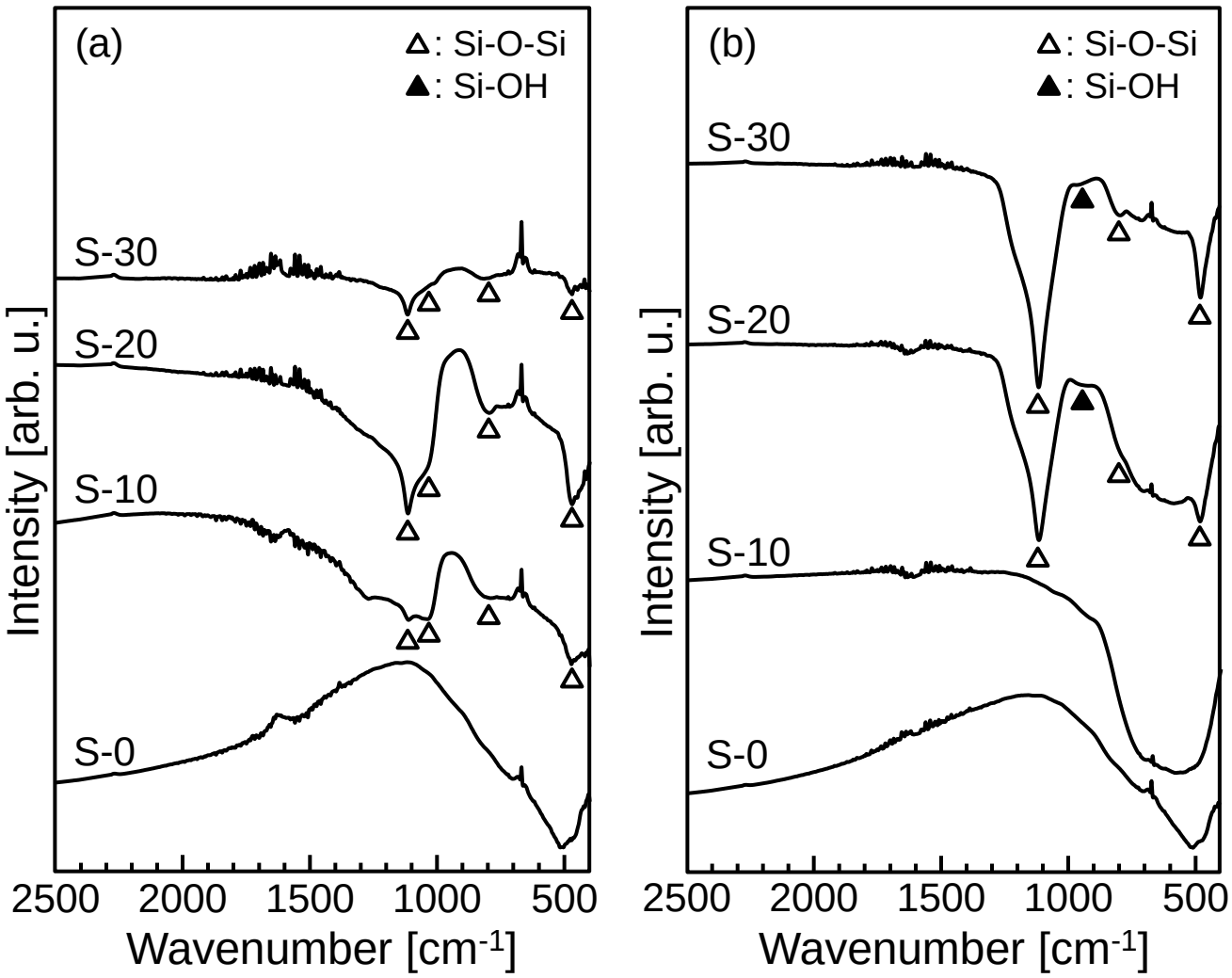

Figure 3
M. Kawashita *et al.*

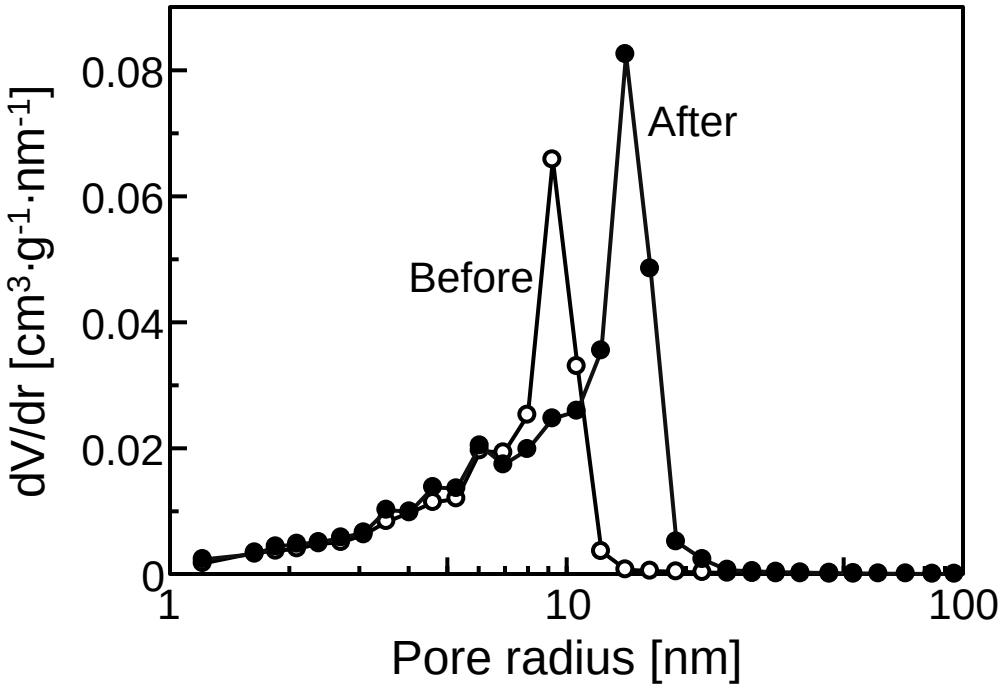

Figure 4
M. Kawashita *et al.*

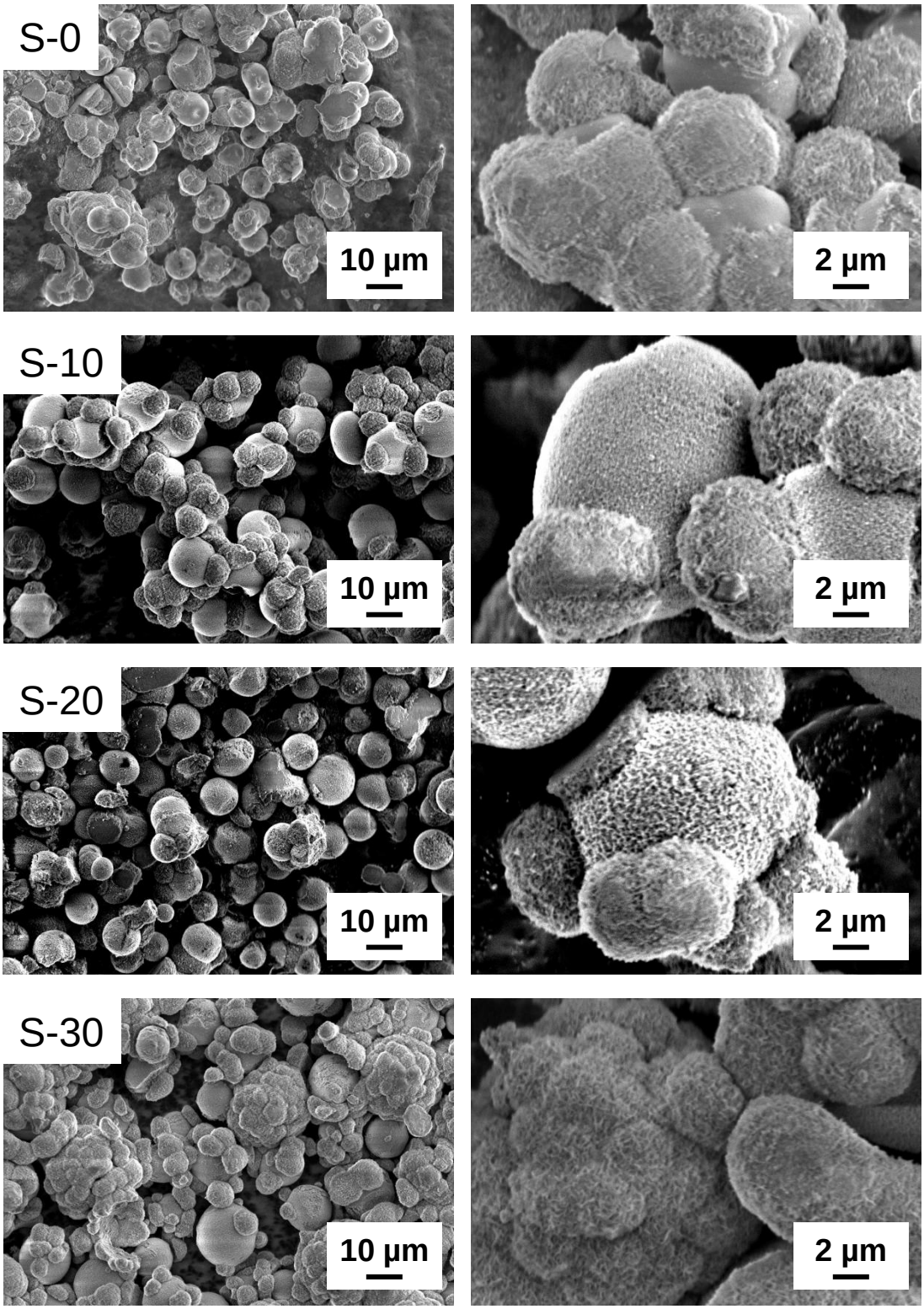

Figure 5
M. Kawashita *et al.*

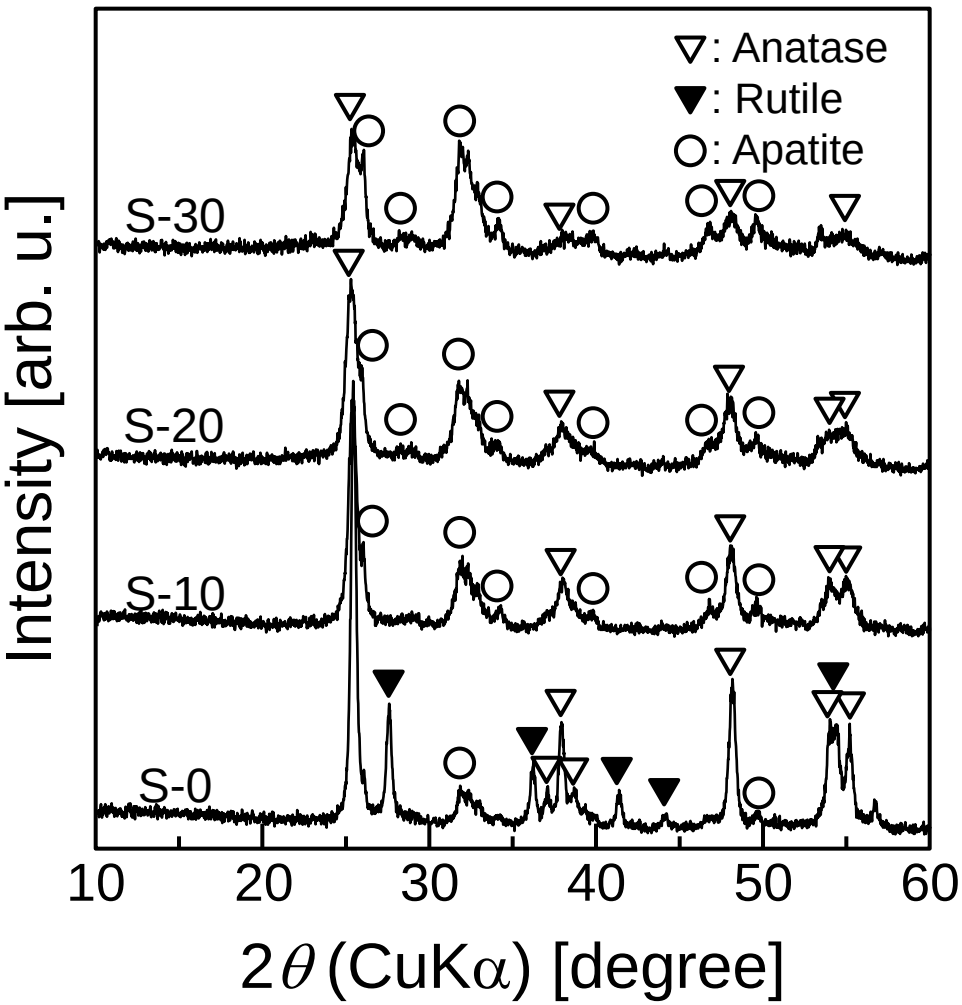

Figure 6
M. Kawashita *et al.*

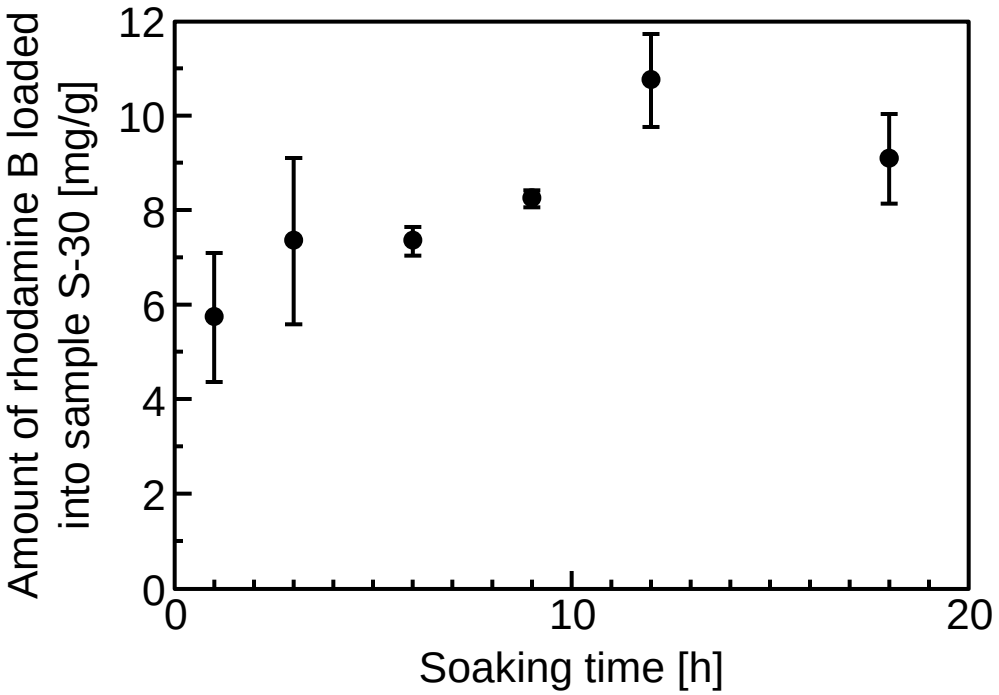

Figure 7
M. Kawashita *et al.*

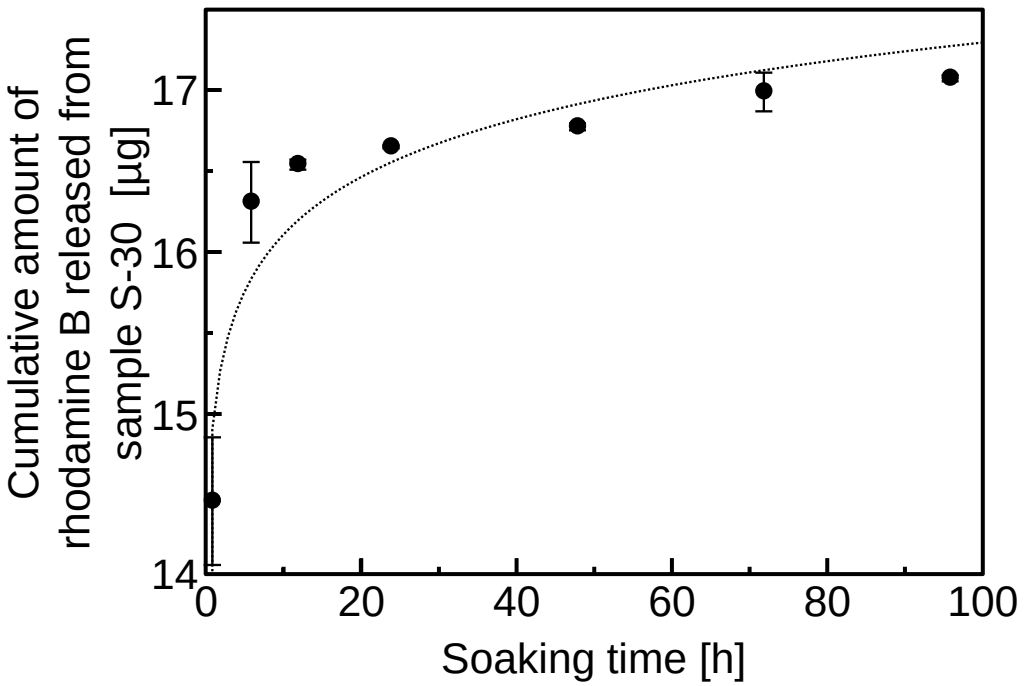

Figure 8
M. Kawashita *et al.*

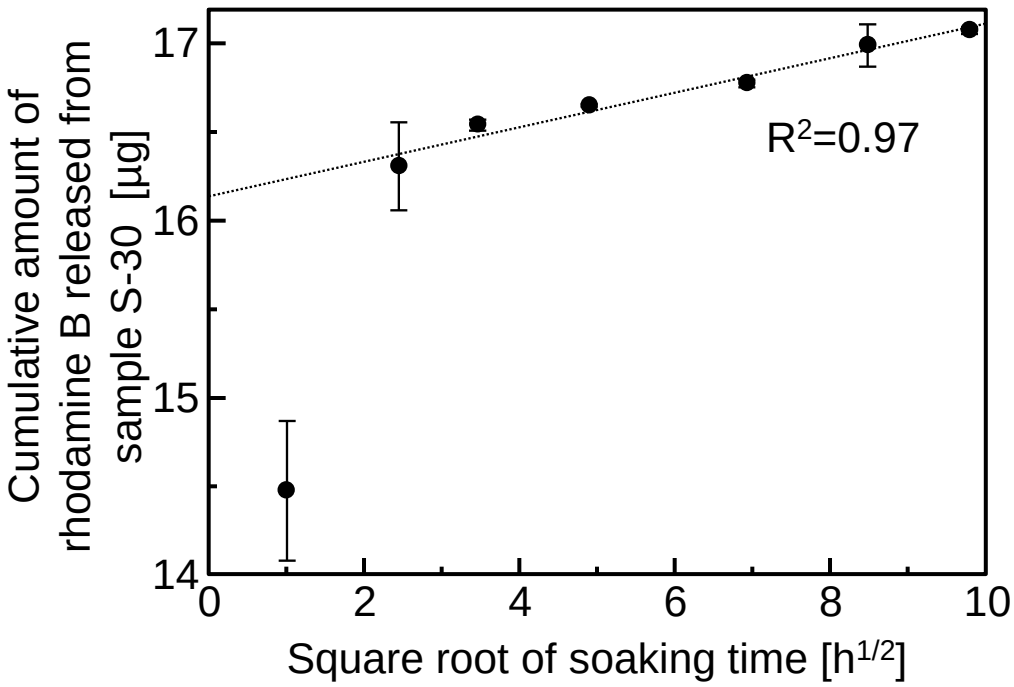

Figure 9
M. Kawashita *et al.*

Table 1 Sample names, amounts of colloidal SiO_2 and H_2O and SiO_2/H_2O weight ratio in the SiO_2 nanoparticle suspension

Sample name	S-0	S-10	S-20	S-30
Colloidal SiO_2 [g]	0.000	1.167	2.625	4.500
H_2O [g]	4.200	3.500	2.625	1.500
SiO_2/H_2O [weight ratio]	0/100	10/90	20/20	30/70

Table 2 SSAs and zeta potentials of samples.

Sample	S-0	S-10	S-20	S-30
SSA [$m^2 \cdot g^{-1}$]	14.5	91.2	107.0	111.7
Zeta potential [mV]	-29.9	-26.2	-27.3	-31.2

Supplementary Data

Click here to download Supplementary Data: -MSAW_12_2.pdf